Supplemental Information

for

# Tailored mechanosensitive nanogels release drugs upon exposure to different levels of stenosis

Ceren Kimna [1,2], Bernardo Miller Naranjo [1,2], Franziska Eckert [1,2], Di Fan [1,2], Dario Arcuti [3], Petra Mela [3], and Oliver Lieleg [1,2,*]

[1] School of Engineering and Design, Department of Materials Engineering, Technical University of Munich, Boltzmannstraße15, 85748 Garching, Germany

[2] Center for Protein Assemblies (CPA) and Munich Institute of Biomedical Engineering, Technical University of Munich, Ernst-Otto-Fischer Straße 8, 85748, Garching, Germany

[3] Medical Materials and Implants, Department of Mechanical Engineering and Munich Institute of Biomedical Engineering, TUM School of Engineering and Design, Technical University of Munich, Boltzmannstraße 15, 85748, Garching

*Corresponding author

Prof. Dr. Oliver Lieleg
Center for Protein Assemblies (CPA), Technical University of Munich,
Ernst-Otto-Fischer Str. 8, 85748 Garching, Germany

*e-mail*: oliver.lieleg@tum.de,
phone: +49 89 289 10952, fax: + 49 89 289 10801

*keywords: drug delivery, atherosclerosis, shear-responsive, deformable*

## 1. Heparin quantification

Heparin release from mechanosensitive nanogels and heparin encapsulation efficiency was determined colorimetrically following the protocol described in the reference [1]. A heparin standard curve (**Figure S1**) was obtained by measuring the absorbance behavior (at 620 nm) of mixtures containing 50 µL of an aqueous heparin solution (heparin concentrations were varied from 0.015 mg/L – 0.1 mg/mL) and 50 µL of the cationic dye Azure A (dissolved at 80 µg/mL in water, Alfa Aesar) with a spectrometer (Molecular Devices SpectraMax ABS, Sunnyvale, CA, USA).

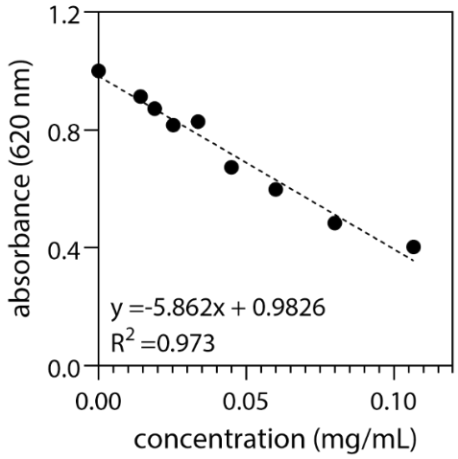


**Figure S1.** Standard curve relating the absorbance properties of serially diluted heparin solutions to their concentration.

## 2. Adjusting the size of the nanogels

As the polymer concentration used for particle generation strongly affects the mechanical rigidity of polymeric nanoparticles, this also leads to strong alterations in the swelling behavior of the polymer matrix. This, in turn, makes it a bit trickier to maintain a constant particle size when varying the composition of the polymer matrix. Here, the hydrodynamic size of the generated nanoparticles was kept in a comparable range by adjusting the volume of the continuous phase during the particle generation step. In brief, when the volume of the continuous phase was initially set to 7.5 mL, it was observed that the hydrodynamic size of the nanogels increased with increasing polymer concentrations (**Figure S2, left**). However, when the polymer concentration was kept constant (10 % PEGDA) and the continuous phase volume was reduced to 5 mL, the average hydrodynamic size of the particles was decreased from 215 ± 50 nm to 400 ± 10 nm. Thus, to obtain nanogels that differ in mechanical properties but have comparable sizes, the volume of the continuous phase was adjusted as follows: 7.5 mL for 10 % PEGDA; 10 mL for 20 % PEGDA, 15 mL for 30 % PEGDA; and 20 mL for 40 % PEGDA nanogels. Indeed, with this strategy, a set of particles with comparable average sizes was obtained (**Figure S2, right**).

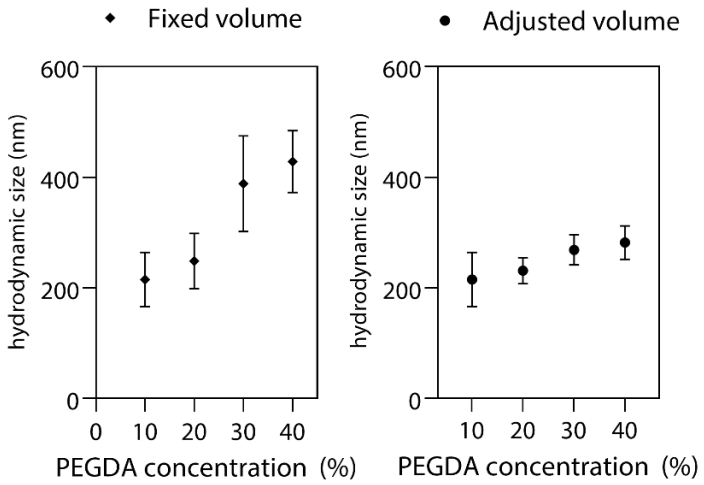


**Figure S2.** Dynamic Light Scattering (DLS) measurements demonstrate that the nanogel size can be tuned by adjusting the volume of the continuous phase. Data shown represents mean values, error bars denote the standard deviation as obtained from $n = 5$ independent samples.

### 3. Stability of the nanogels

The stability of the PEGDA nanogels was analyzed under storage conditions, where the nanoparticles were incubated in PBS (pH = 7.4) at 4 °C (in the absence of shear forces) for 3 weeks. As summarized in **Figure S3,** the hydrodynamic size and the polydispersity index (PDI) of the different nanogels showed only slight variation, indicating their good stability in the absence of mechanical challenges.

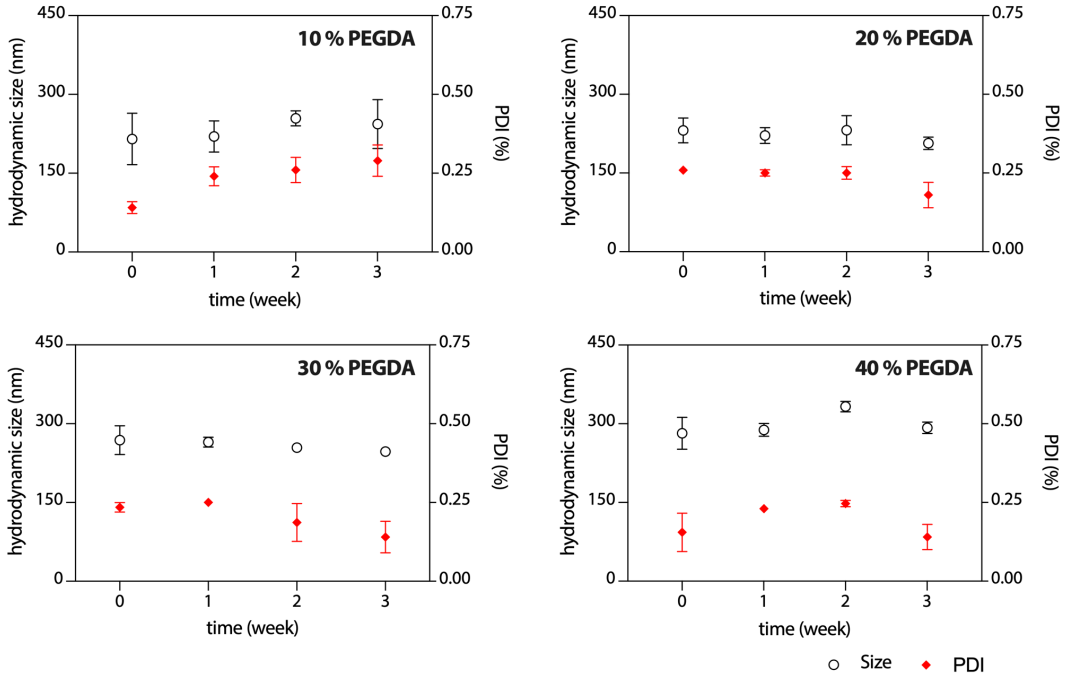


**Figure S3.** Dynamic Light Scattering (DLS) measurements demonstrate the good stability of nanogels over a time span of 3 weeks. Data shown represents mean values, error bars denote the standard deviation as obtained from $n = 5$ independent samples.

## 4. Gelation kinetics of PEDGA samples in response to UV light

Rheological measurements that follow the viscoelastic moduli (*G'*, *G"*) of macroscopic PEGDA samples over time reveal that once exposed to UV light; all tested PEGDA formulations rapidly change from the state of a viscoelastic solution to the state of a viscoelastic solid (**Figure S4**). This verifies the success of the UV-based cross-linking strategy we here apply to stabilize the different PEGDA matrices.

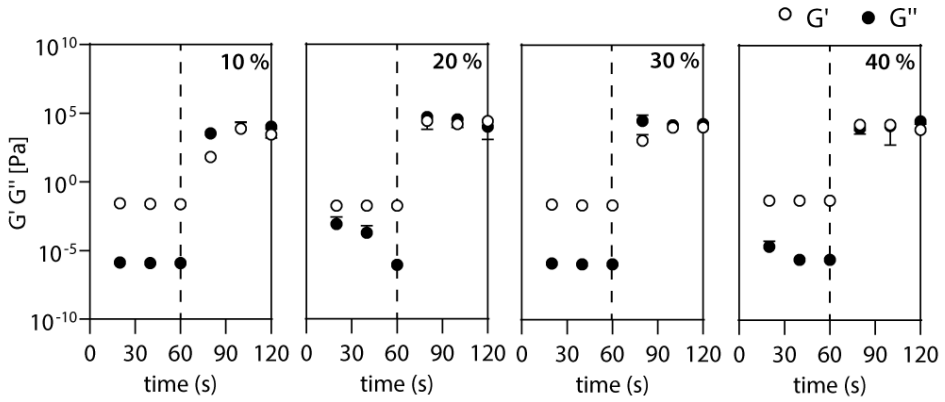


**Figure S4.** Gelation curves of the different PEGDA samples. Dashed lines indicate where the UV illumination was initiated (*i.e.*, at $t = 60$ s). Data shown represents mean values, error bars denote the standard deviation as obtained from $n = 5$ independent samples.

## 5. Swelling behavior of macroscopic PEGDA gels

To determine the swelling behavior of the different PEGDA gels, macroscopic samples were prepared as described in the Methods section of the main text. Their weight was determined, and then they were immersed into PBS (pH = 7.4). At predetermined time intervals, the samples were weighted to calculate their swelling ratio. After 72 h of immersion in PBS, the determined swelling ratios of the samples varied between 4 – 20 % (**Figure S5**). Importantly, the swelling ratio increased when increasing the polymer concentration in the gels.

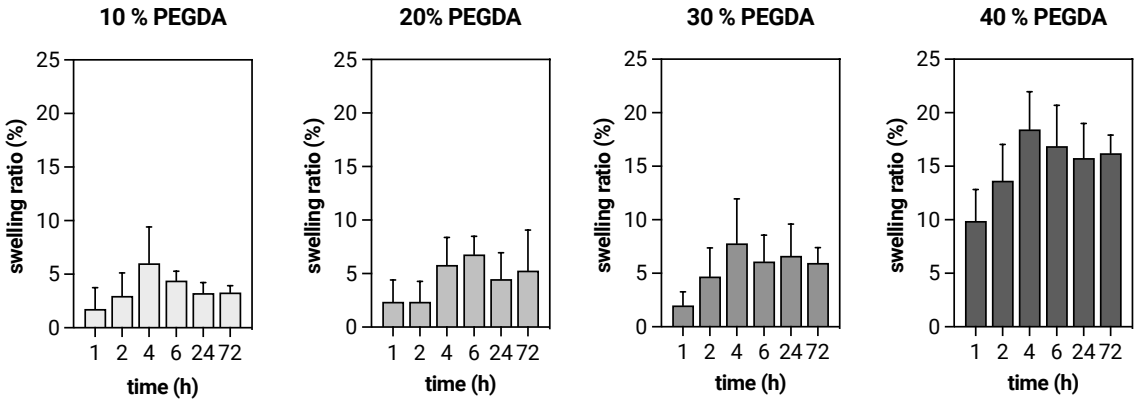


**Figure S5.** Swelling ratios of macroscopic, 10 % – 40 % PEGDA gels when immersed in 1x PBS (pH = 7.4). Data represents mean values; error bars denote the standard deviation as obtained from n ≥ 4 samples.

## 6. Microfluidic experiments with fluorescently labeled nanogels

Fluorescent rhodamine B was added to the water phase during the PEGDA particle formation process, as described in the main text. The nanogels were imaged as described in the Methods section of the main text.

For each nanogel sample, after having passed on of the microchannels (reference channel: no stenosis; test channels: 70% and 90% stenosis, respectively), fluorescent images were acquired from 5 independent locations, and the total number of nanogels determined from those 5 images was calculated by using the software ImageJ. The results of those tests are compiled in **Figure S6**.

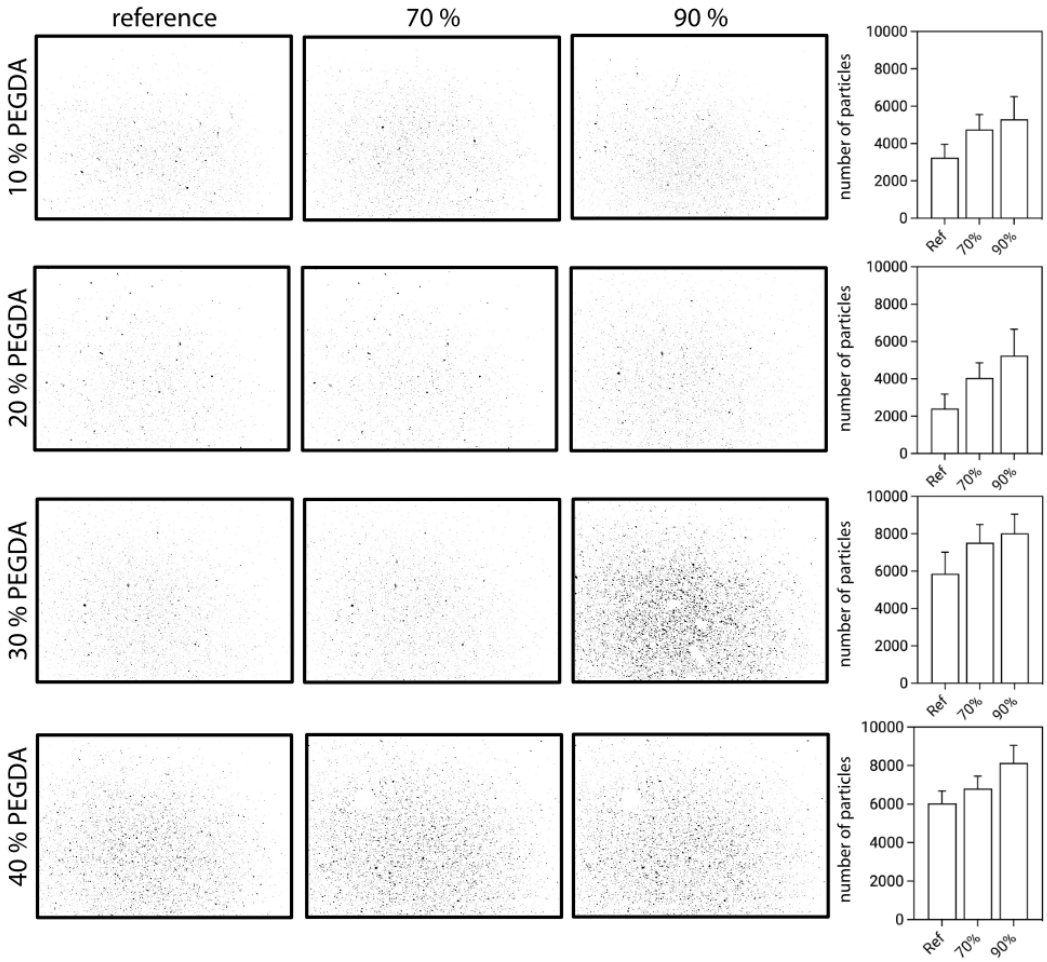


**Figure S6.** Representative images and the determined number of fluorescently labeled nanogels after they passed through microchannels of different stenosis levels. The number of nanogels shown in the bar plots was determined from 3 independent experiments; in each experiment, 5 images obtained from different locations of the collected sample were analyzed. Data shown represents mean values, error bars denote the standard deviation.

In addition, the fluorescence bulk intensity of a 30 % PEGDA nanogel sample flushed through different microchannels was quantified using a Fluoroskan Ascent ® FL plate reader (Thermo Scientific; Ex/Em = 390/510). No statistically significant difference in the bulk fluorescence intensity was detected between groups that passed different channels (reference: no stenosis; test channels:

70% and 90% stenosis, respectively), and no statistically significant difference in the bulk fluorescence intensity was detected (**Figure S7**). This indicates that the nanogels were not trapped in the stenotic regions of the microchannels.

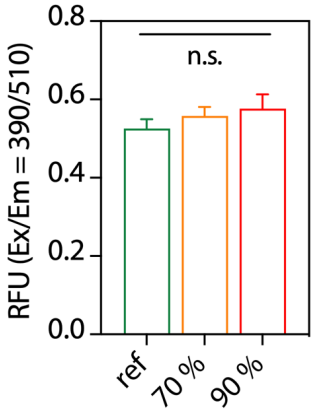


**Figure S7.** Fluorescence bulk intensity of 30 % PEGDA nanogel samples after they passed microfluidic channels with different stenosis levels. To avoid variations in the nanogel concentration, those measurements were performed with the same batch of nanoparticles. Data shown represents mean values, and error bars denote the standard deviation as obtained from $n = 5$ independent tests each.

## 7. Assessing the influence of the amine-modification on the material characteristics of PEGDA gels

The effect of the amine modification (described in the main text) on material characteristics of PEDGA gels was tested by comparing selected properties of 30 % PEGDA-$NH_2$ macro- and nanogels with those of their unmodified PEGDA counterparts.

***Bulk rheology:*** **Figure S8** depicts gelling kinetics, linear viscoelastic moduli (determined at a frequency of $f = 1$ Hz) as well as an assessment of the non-linear behavior (LAOS measurements) of macroscopic 30 % PEGDA (left) and 30% PEGDA-$NH_2$ (right) gels. After gelation, the loss and storage moduli (at $f = 1$ Hz) show no statistical significance. Similarly, strain weakening sets in at the ~8$^{th}$ measurement points for both PEGDA variants (with and without amine-modification).

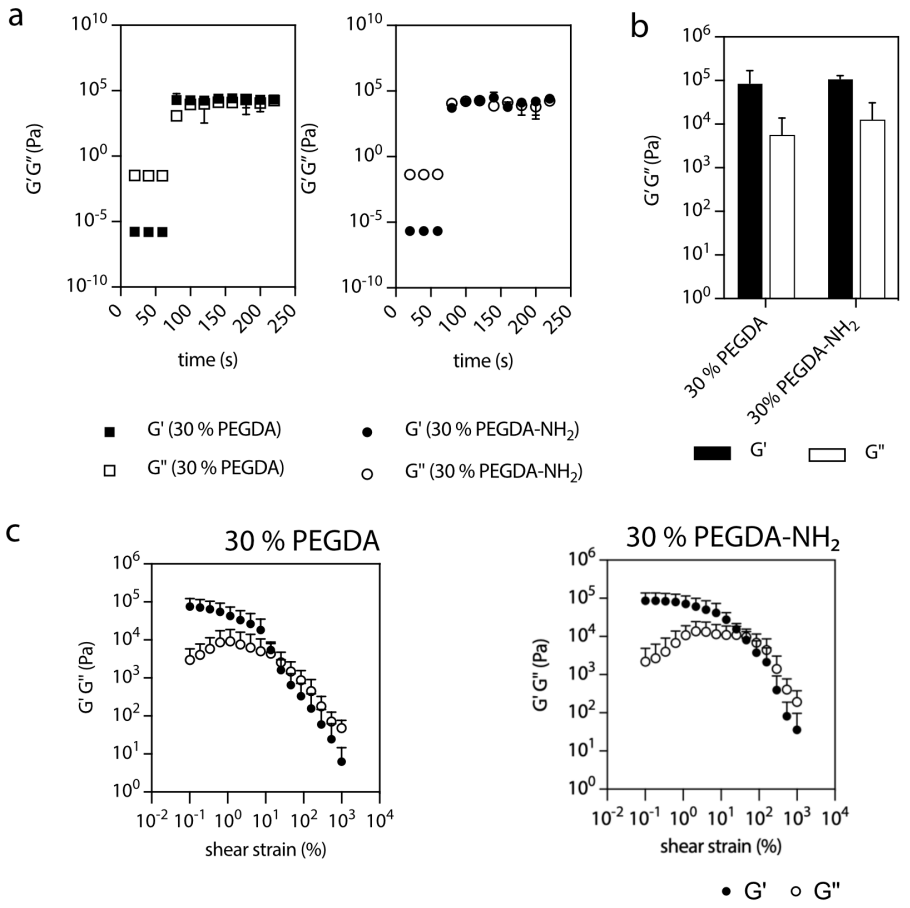


**Figure S8.** (**a**) Gelation curves of macroscopic 30 % PEGDA and 30 % PEGDA-$NH_2$ gels. UV illumination starts at $t$ = 60 s. (**b**) Viscoelastic moduli of 30 % PEGDA and 30 % PEGDA-$NH_2$ gels after UV crosslinking (values were determined at $f$ = 1 Hz). (**c**) Non-linear viscoelastic properties as determined by LAOS strain sweeps. All data shown represents the mean of $n$ = 3 independent samples. Error bars denote the standard deviation.

***Response of nanogels to macroscopic shear stress and triggered nanogel dispersal in microfluidic channels:*** After generating 30 % PEGDA-$NH_2$ nanogels (which was conducted as described in the main text), their response to macroscopic shear stress (**Figure S9,** left) as well as their response to different microchannels (**Figure S9,** right; reference channel: no stenosis; test channels: 70 % and 90 % stenosis, respectively) was determined as described in the respective methods section of the main text. Moreover, findings obtained upon exposure to macroscopic (rheology) and microscopic (microfluidic stenosis) shear stress do not remarkably differ from those obtained with unmodified 30 % PEGDA nanogels.

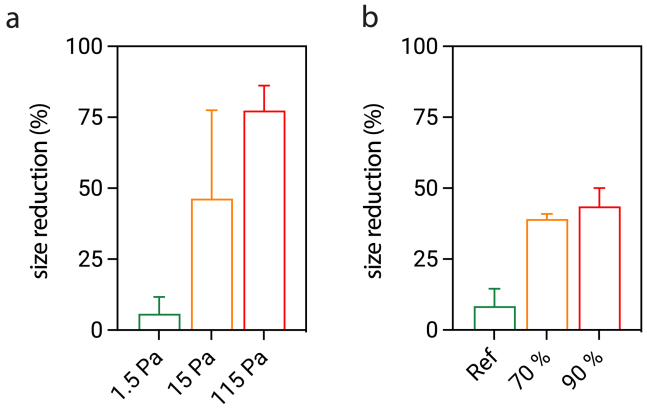


**Figure S9.** (**a**) Size reduction of 30 % PEGDA-$NH_2$ nanogels after the application of different macroscopic shear stress levels. (**b**) Shear-dependent size reduction of 30 % PEGDA-$NH_2$ nanogels after passing them through microchannels of different stenosis levels. Data shown represents mean values; error bars denote the standard deviation as obtained from $n = 3$ independent samples.

### 8. *In vitro* cytotoxicity tests performed with fibroblast cells

Fibroblasts (NIH/3T3) were cultured in Dulbecco's modified Eagle medium (DMEM; Sigma-Aldrich) supplemented with 10 % fetal bovine serum (FBS; Sigma-Aldrich), and incubated at 37 °C in a humidified atmosphere with 5 % $CO_2$, until 95 % confluency was reached. The viability of cells after incubation with 40 % PEGDA nanogels (either unmodified or amine-modified ones) was evaluated by employing a WST-1 assay (Sigma Aldrich) as described in the main manuscript. Similar to the results obtained with HUVEC cells, also NIH/3T3 cells showed > 85 % viability at all tested nanogel concentrations (**Figure S10**).

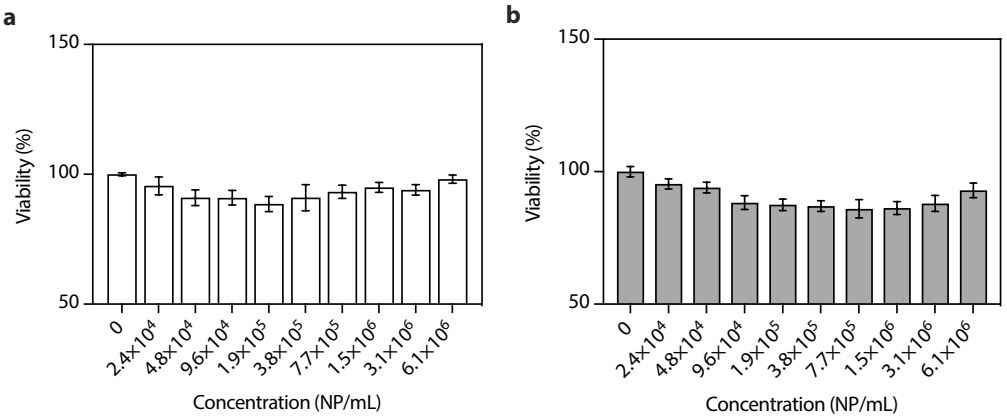


**Figure S10.** *In vitro* viability of NIH/3T3 cells incubated with unmodified (**a**) and $NH_2$-modified (**b**) 30 % PEGDA nanogels, respectively. Data shown represents mean values, and error bars denote the standard deviation ($n = 6$).

## 9. Nanogel stability in platelet poor plasma

To assess the biological stability of the nanogels in blood plasma, platelet poor plasma was collected (as described in the Methods section of the main text) and used as an incubation medium for the nanogels to test for putative changes in their size distribution. In detail, we tested amine modified variants of the 10 % PEGDA and 40 % PEGDA nanogels. After the last washing step (see the Methods section for the nanogel preparation), the samples were dispersed in 2 mL of platelet poor plasma and placed into a temperature controlled shaking incubator (37 °C) operating at 40 rpm. At predetermined time intervals (*i.e.*, 1 – 5 h; days 1 - 5), 850 µL of a sample was removed and analyzed using a Litesizer500 (Anton Paar) to assess the hydrodynamic size and the polydispersity index. The obtained results indicated that incubation in platelet poor plasma did not induce any aggregation or degradation of the nanogels studied here (**Figure S11**).

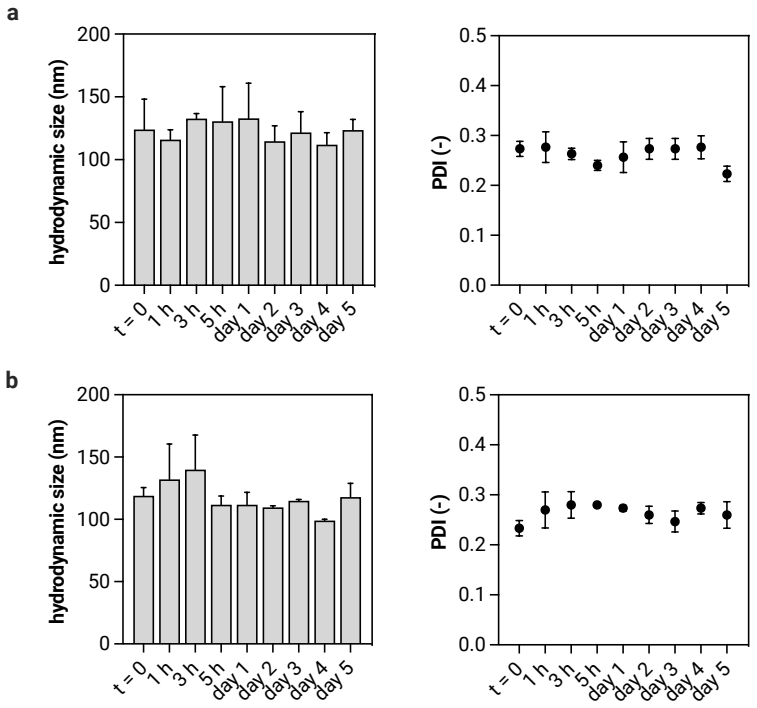


**Figure S11.** Hydrodynamic size and PDI of 10 % PEGDA (**a**) and 40 % PEGDA (**b**) nanogels when incubated in platelet poor plasma at 37 °C. Data represents mean values and error bars denote the standard deviation as obtained from $n = 3$ samples.

## 10. Mechanosensitive properties of nanogels in a blood environment

We assessed the mechanosensitive properties of nanogels in a blood environment. To do so, (fluorescently labeled) 30 % PEGDA nanogels (with and without -$NH_2$ modification) were prepared as described in the *Materials and Methods* section of the manuscript. Then, 100 µL of the nanogel dispersion was mixed with 500 µL of a human blood sample. Next, the nanogel dispersions were flushed through three different microchannels with different levels of stenosis (*i.e.*, no stenosis, 70 %, and 90 % stenosis), and the number of nanogels was quantified as described in the main text. As

the results summarized in **Figure S12** show, the nanogels also display a stenosis-dependent mechanosensitive behavior in the complex environment of human blood.

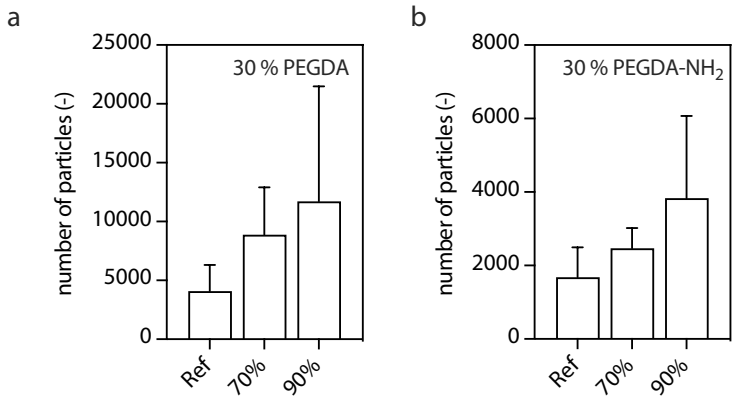


**Figure S12.** Number of fluorescently labeled (**a**) 30 % PEGDA and (**b**) 30% PEGDA-$NH_2$ nanogels dispersed in a human blood sample after they passed through microchannels of different stenosis levels. The number of nanogels was determined from 3 independent experiments; in each experiment, 10 images obtained from individual experiments were analyzed. Data shown represents mean values, error bars denote the standard deviation.

### 11. Visualization of heparin loading into nanogels by colocalization tests

To visualize heparin entrapment into the PEGDA nanogels, an amine modified fluorescent dye (Atto488) was conjugated to the heparin molecules *via* carbodiimide chemistry. To visualize the nanogels themselves, PEGDA was labeled with rhodamine B (see the methods section of the main manuscript for details). Then, heparin loaded nanogels were placed onto a counting chamber and imaged using an upright microscope (Axioskop 2 Mat microscope, Zeiss, Oberkochen, Germany) equipped with FITC and rhodamine filters (Zeiss). In the obtained images, the green signal represents (fluorescently labeled) heparin, whereas the red signal shows the PEGDA polymer. As shown in **Figure S13**, the two signals overlap, and a yellow/orange color is visible when the fluorescent images are merged. This finding shows that heparin loading into the PEGDA nanogels was successful.

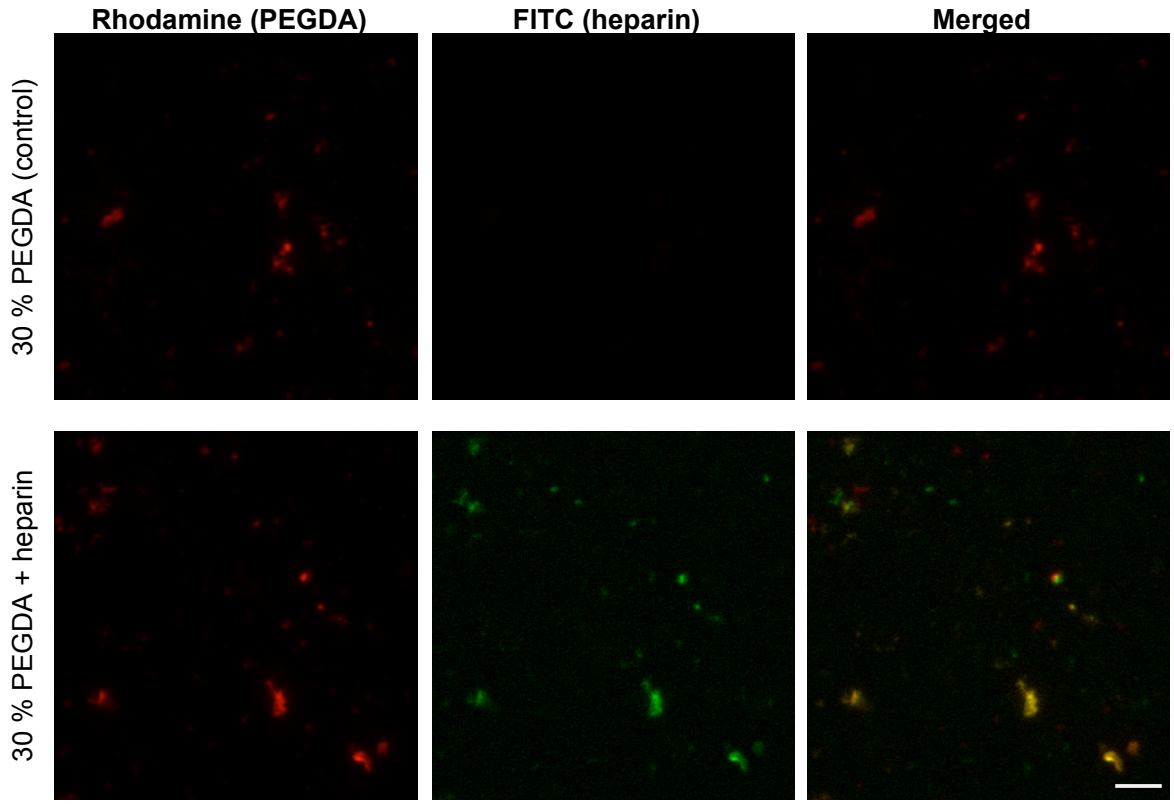


**Figure S13.** Colocalization of heparin (green) and PEGDA polymers (red) in the nanogels. The scale bar represents 10 µm, and applies to all images.

### 12. NP behavior in hypertension

To test whether an increased static pressure leads to NP breakup, we built a pressure chamber using a conventional Luer-Lock 10 mL syringe (B. Braun Melsungen AG, Melsungen, Germany) and a 2-way Luer-Lock valve (Carl Roth GmbH & Co. KG, Karlsruhe, Germany). We filled the syringe with 1 mL of NP solution and 8 mL of air; we assumed the NP solution to be incompressible and the air to behave like an ideal gas. We then compressed the air by 2 mL to create an overpressure of 28,700 Pa (225 mmHg), which corresponds to a level of pressure found in patients with critical vascular hypertension. Then, we measured the size distribution of two NP variants (the softest and the hardest variants, *i.e.*, 10% and 40% PEDGA) before and after exposing them to this overpressure for 1 h. As shown in **Figure S14**, we found that such a static pressure application does not affect the NP size on the time scale tested by us. This suggests that the NPs should be reasonably stable when used in patients with hypertension.

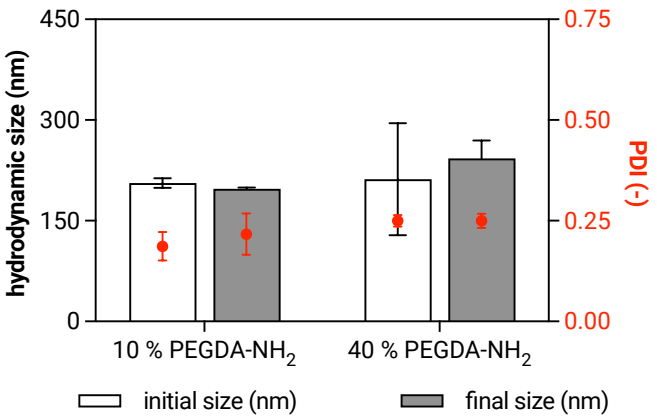


**Figure S14.** Hydrodynamic size of 10 % PEGDA (soft) and 40 % PEGDA (hard) nanogels before and after exposure to an elevated pressure of 130.000 Pa ($n = 3$). Data represents mean values; error bars denote the standard deviation.

With those findings in mind, we then conducted a series of additional simulations using the CAD and CFD models described in the main paper as a basis. First, we increased the static pressure in the 70 % stenosis model (**Figure S15 b**) while keeping all other parameters (including the flow velocity) unchanged. The such obtained results showed that a static pressure increase itself does not affect the wall shear stress (WSS); this matches our expectation (since the WSS depends on the velocity profile of the flow) and agrees with the experimental results discussed above.

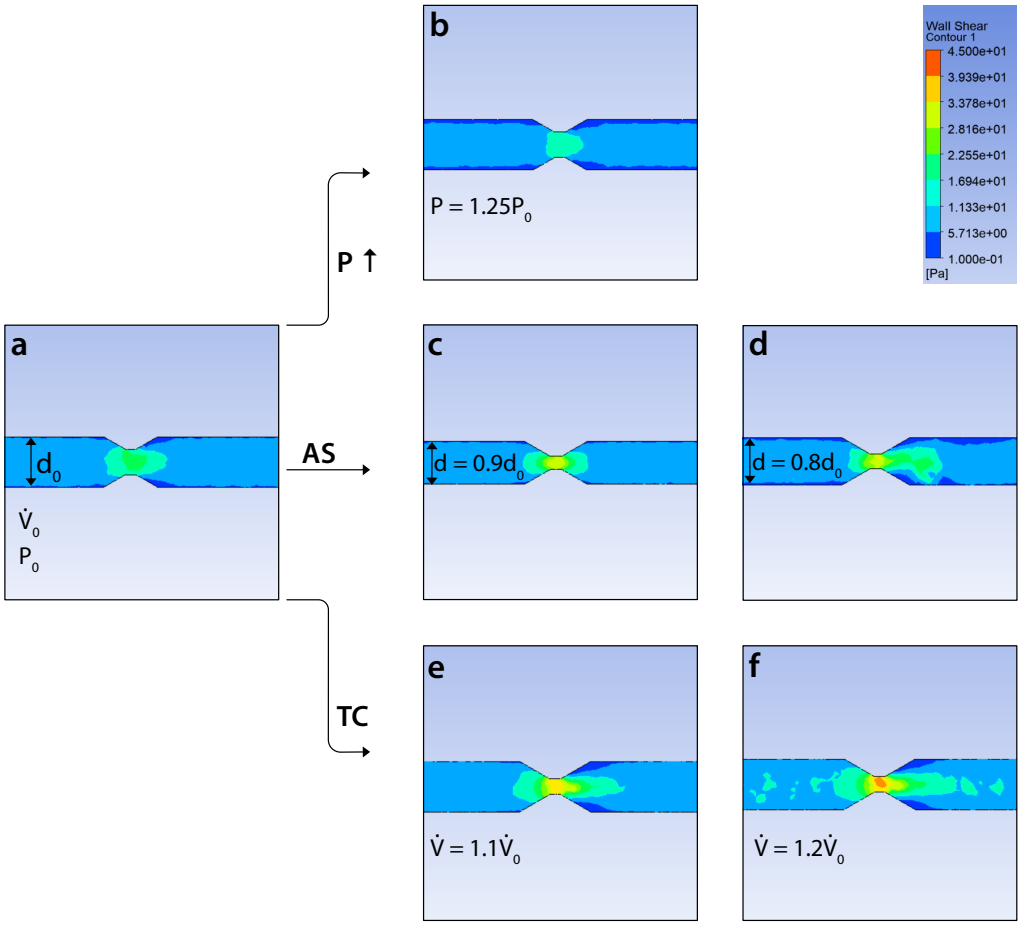


**Figure S15**. Simulation results of a parameter analyze the effect of increased pressure (*P*), vessel diameter (*d*) and blood flow rate ($\dot{V}$) on the WSS the NPs experience in a microchannel. Compared to standard conditions in a 70% constriction (**a**, see main text), an increase of the static pressure by 25,000 (~180 mmHg) does not perceivably change the WSS levels. **c,d**) Reduced channel diameters (a reduction by 10 % and 20 %, respectively; this is supposed to mimic a reduced blood vessel elasticity as typical in atherosclerosis, AS) lead to higher flow velocities. **e,f**) Increased blood flow rates (to model tachycardia, TC) cause an increase in flow velocity as well. The color code in the upper right corner applies to all subfigures.

Physiologically, there can be various reasons leading to hypertension, and it is very difficult (if not impossible) to discuss them all here (in many cases, it is not clear how the physical parameters in the blood circuit are affected in those pathological conditions leading to hypertension). However, in a next step, we identified two examples of pathological conditions, which are known to lead to hypertension, *i.e.*, atherosclerosis and tachycardia, and where information is available how the physical properties of the blood flow are altered.

*Atherosclerosis:* In patients suffering from atherosclerosis, the blood vessels are stiffer than in healthy individuals. If we consider that this increase in vessel stiffness might lead to smaller vessel diameters and keep the cardiac output (CO) unchanged, atherosclerotic conditions should translate into higher blood flow velocities and therefore higher WSS. To test this idea, we reran a set of simulations on the 70% stenosis channel and now narrowed the channel main diameter in two steps: first, by 10%;

second, by 20%. In both cases, we adapted the flow velocity to keep the volume flow the same as in the original channel. As expected, the results show that the narrowing of the vessels entails an increase in flow velocity and thus higher levels of WSS (see **Figures S15 c,d**). For the mechanosensitive nanogels studied here, this means that one should expected enhanced drug release from the nanogels (compared to non-hypertension conditions) caused by an increased NP disintegration.

*Tachycardia:* In patients suffering from tachycardia, hypertension is created by an increased heart rate. Thus, for modelling this particular scenario, we assumed an increased CO while keeping all other parameters unchanged. To implement this modification into the simulations, we again selected the 70% stenotic channel and increased the volume flow by 10 % and 20 %, respectively. When doing so, we observed, again fully in line with our expectations, larger flow velocities and thus larger WSS (see **Figure S15 e,f**). In other words, also in hypertension conditions caused by tachycardia, we would expect our nanogels to break-up and release their cargo with higher efficiency than at normal blood pressure.

However, in both scenarios, the increased NP dispersal does not directly originate from the increased blood pressure itself but from the increased WSS levels resulting from the detailed pathophysiological setting.

**References**

1 Warttinger, U., Giese, C. & Krämer, R. Comparison of Heparin Red, Azure A and Toluidine Blue assays for direct quantification of heparins in human plasma. *arXiv preprint arXiv:1712.03377* (2017).